

# Frustrated Superconductivity in the Trilayer Nickelate $\text{La}_4\text{Ni}_3\text{O}_{10}$

Qiong Qin,<sup>1,2</sup> Jiangfan Wang,<sup>3</sup> and Yi-feng Yang<sup>1,2,4,\*</sup>

<sup>1</sup>*Beijing National Laboratory for Condensed Matter Physics and Institute of Physics, Chinese Academy of Sciences, Beijing 100190, China*

<sup>2</sup>*University of Chinese Academy of Sciences, Beijing 100049, China*

<sup>3</sup>*School of Physics, Hangzhou Normal University, Hangzhou, Zhejiang 311121, China*

<sup>4</sup>*Songshan Lake Materials Laboratory, Dongguan, Guangdong 523808, China*  
(Dated: May 8, 2024)

Motivated by the opposite trend of maximum  $T_c$  in multilayer nickelate and cuprate superconductors, we propose an interlayer pairing scenario for the superconductivity of the trilayer nickelate  $\text{La}_4\text{Ni}_3\text{O}_{10}$  discovered recently under high pressure. Our theory reveals intrinsic frustration of the spin-singlet pairing formed between two outer layers and the same inner layer, which causes strong superconducting fluctuations between layers and thus explains the reduction of its maximum  $T_c$  compared to that of the bilayer  $\text{La}_3\text{Ni}_2\text{O}_7$ . This supports a fundamental distinction between multilayer nickelate and cuprate superconductors associated with their potentially different (interlayer vs intralayer) pairing mechanisms. Our theory predicts extended  $s^\pm$ -wave gap structures in  $\text{La}_4\text{Ni}_3\text{O}_{10}$ , with varying signs and possible nodes on different Fermi pockets. We also find an intrinsic Josephson coupling with potentially interesting consequences to be examined in future experiments.

*Introduction.*—The recent discoveries of superconductivity in bilayer [1–3] and trilayer [4–8] nickelates under high pressure have stimulated intensive experimental [9–21] and theoretical [22–73] debates concerning their pairing mechanisms as well as potential connections with the cuprate high-temperature superconductivity. While in-plane pairing has been well established in cuprates, both interlayer and intralayer pairing scenarios have been proposed to explain the superconductivity in bilayer and trilayer nickelates. Latest resonant inelastic X-ray scattering (RIXS) measurements on  $\text{La}_3\text{Ni}_2\text{O}_7$  at ambient pressure [17] reported a dominant interlayer superexchange interaction  $J$ , which seems to support the interlayer scenario, but a straightforward experimental confirmation is still difficult due to the high pressure.

In this work, we point out that the different variation of the maximum  $T_c$  in multilayer cuprate and nickelate superconductors might be an indicator of their possibly distinct pairing mechanisms. In cuprates, the maximum  $T_c$  is the highest in trilayer systems. At ambient pressure, it rises from 97 K (single layer) to 135 K (trilayer) in Hg-based cuprates and from 30 K to 115 K in Bi-based cuprates [74, 75]. By contrast, the maximum  $T_c$  is reduced from about 80 K in the bilayer nickelate  $\text{La}_3\text{Ni}_2\text{O}_7$  to about 30 K in the trilayer nickelate  $\text{La}_4\text{Ni}_3\text{O}_{10}$ . To understand this difference, we perform numerical simulations on an effective low-energy model of the trilayer nickelate and find for interlayer pairing a maximum ratio  $T_c/J \approx 0.02 - 0.03$ , which is reduced by nearly a half compared to that of  $0.04 - 0.05$  in the bilayer model [44]. We show that the reduction is caused mainly by strong superconducting fluctuations induced by some intrinsic frustration of the interlayer pairing fields that is absent for intralayer pairing, while imbalance between the inner and two outer layers may further suppress  $T_c$  in the trilayer structure. An intrinsic Josephson coupling

is also revealed that may have potentially interesting consequences to be examined in future experiments.

*Model and method.*—We start with the following low-energy effective two-orbital trilayer model based on experimental and first-principles considerations [10, 72, 76],

$$H = - \sum_{lij s} (t_{ij} + \mu \delta_{ij}) c_{lis}^\dagger c_{ljs} - \sum_{lij} V_{ij} (c_{lis}^\dagger d_{ljs} + h.c.) - t_\perp \sum_{ais} (d_{0is}^\dagger d_{ais} + h.c.) + J \sum_{ai} \mathbf{S}_{0i} \cdot \mathbf{S}_{ai}, \quad (1)$$

where  $d_{lis}$  ( $c_{lis}$ ) is the annihilation operator of  $d_{z^2}$  ( $d_{x^2-y^2}$ ) electrons with spin  $s$  on site  $i$  of the inner ( $l = 0$ ) or two outer ( $l = \pm$ ) layers,  $\mathbf{S}_{li} = \frac{1}{2} \sum_{ss'} d_{lis}^\dagger \boldsymbol{\sigma}_{ss'} d_{lis}$  is the  $d_{z^2}$  spin density operator with  $\boldsymbol{\sigma}$  being the Pauli matrices, the subscript  $a = \pm$  denotes two outer layers,  $t_{ij}$  and  $\mu$  are the in-plane nearest-neighbor hopping and the chemical potential of  $d_{x^2-y^2}$ ,  $V_{ij}$  is the renormalized in-plane hybridization between nearest-neighbor  $d_{z^2}$  and  $d_{x^2-y^2}$  orbitals satisfying  $V_{i,i+\hat{x}} = -V_{i,i+\hat{y}} = V$ ,  $t_\perp$  is the renormalized interlayer hopping of  $d_{z^2}$  quasiparticles, and  $J$  is the  $d_{z^2}$  interlayer superexchange interaction mediated by apical oxygens. Other small parameters are ignored for simplicity. The effect of the Hund's rule coupling is absorbed in the renormalized hybridization  $V$  which is set as a free tuning parameter [32, 40]. The intralayer superexchange interaction is small as reported in latest RIXS and inelastic neutron scattering (INS) measurements [16, 17], and thus ignored to focus on interlayer pairing only.

We employ the static auxiliary field Monte Carlo approach that has been widely applied to strongly correlated electron studies [77–88]. Its application to the bilayer nickelate superconductor has predicted the evolution of  $T_c$  in good consistency with experiment [44]. To simulate the trilayer model, we decouple the superex-

change term [89]:

$$J\mathbf{S}_{0i} \cdot \mathbf{S}_{ai} \rightarrow \sqrt{2}\bar{\Delta}_i^a \Phi_i^a + \sqrt{2}\bar{\Phi}_i^a \Delta_i^a + \frac{8\bar{\Delta}_i^a \Delta_i^a}{3J}, \quad (2)$$

where  $\Phi_i^a = \frac{1}{\sqrt{2}}(d_{0i\downarrow}d_{ai\uparrow} - d_{0i\uparrow}d_{ai\downarrow})$  denotes the local interlayer  $d_{z^2}$  spin singlet at site  $i$  between the inner and  $a$ -th outer layers, and  $\Delta_i^a$  is its corresponding pairing field. The static approximation ignores the imaginary time dependence of the auxiliary fields,  $\Delta_i^a(\tau) \rightarrow \Delta_i^a = |\Delta_i^a|e^{i\theta_i^a}$ , to avoid the severe sign problem, while the full thermodynamic fluctuations are retained beyond the uniform mean-field approximation. Hence, it is particularly suitable for studying the Berezinskii-Kosterlitz-Thouless (BKT) transition in two-dimensional superconductivity at finite temperatures [90–92].

We first integrate out all fermionic degrees of freedom to obtain an effective action solely of the pairing fields:

$$S_{\text{eff}}(\{\Delta_i^a\}) = \frac{8\beta}{3J} \sum_{ia} \bar{\Delta}_i^a \Delta_i^a - \sum_i \ln(1 + e^{-\beta\tilde{\Lambda}_i}) - \sum_i \ln(1 + e^{-\beta\Lambda_i}), \quad (3)$$

where  $\tilde{\Lambda}_i$  and  $\Lambda_i$  are the eigenvalues of two matrices determined by the tight-binding parameters and the pairing configuration  $\{\Delta_i^a\}$  [93]. Monte Carlo simulations are then performed to sample the probability distribution  $p(\{\Delta_i^a\}) = Z^{-1}e^{-S_{\text{eff}}(\{\Delta_i^a\})}$ , where  $Z$  is the partition function serving as a normalization factor. Hereafter, we will set  $t$  to unity as the energy unit and fix the chemical potential  $\mu = -1.3$  so that the total electron density only varies slightly around its nominal value 2.67. Due to computational limitation, all presented results are obtained on a  $10 \times 10$  trilayer lattice but the conclusions have been examined to be robust with other lattice sizes.

*Reduction of  $T_c$ .*—Theoretically, the BKT transition is characterized by a rapid increase of the vortex number  $n_v$  [94]. Figure 1(a) plots its temperature derivative  $dn_v/dT$  for three different values of  $V$  at fixed  $J = 0.5$  and  $t_{\perp} = 0$ . A peak is clearly seen for each curve that defines the temperature scale  $T_c^v$ . To confirm that this indeed marks a superconducting transition, we further calculate the phase mutual information  $I_{\mathbf{R}}$  between two local pairing fields of the largest distance  $\mathbf{R} = (5, 0)$  along the  $x$  direction [44, 95–100]. As shown in Fig. 1(b), the phase mutual information displays several slope changes with lowering temperature in the semilog plot. Its rapid increase at intermediate temperature region marks the development of long-distance phase correlation, with a lower boundary  $T_c^l$  coinciding with  $T_c^v$  determined from the vortex number. We thus identify them as the superconducting transition temperature  $T_c$  at which phase coherence is developed between local pairs on distant interlayer bonds.

Figure 1(c) compares the estimated  $T_c$  for bilayer and trilayer models of the same parameters. Both vary non-

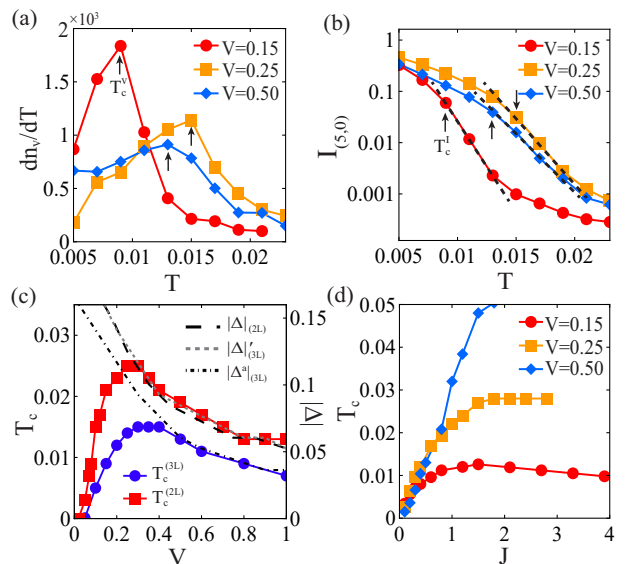


FIG. 1: Temperature evolution of (a) the derivative  $dn_v/dT$  of the vortex number  $n_v$  and (b) the superconducting phase mutual information  $I_{(5,0)}$  for three typical values of the hybridization parameter  $V = 0.15, 0.25, 0.50$  and  $J = 0.5$ . The maximum of  $dn_v/dT$  reflects the BKT transition for two-dimensional superconductivity and defines the temperature scale  $T_c^v$ , and the slope change (dashed lines) in  $I_{(5,0)}$  at low temperatures marks the long-distance phase coherence and defines the temperature scale  $T_c^l$ . They together define the superconducting transition temperature  $T_c$ . (c) Comparison of  $T_c$  for trilayer and bilayer models as functions of the hybridization  $V$  at  $J = 0.5$ . Also shown are the most probable values of the pairing amplitudes  $|\Delta^a|$  and  $|\Delta|' = \sqrt{|\Delta^+|^2 + |\Delta^-|^2}$  of the trilayer model and  $|\Delta|$  of the bilayer model. (d) Evolution of the trilayer  $T_c$  as functions of the interlayer superexchange interaction  $J$  for  $V = 0.15, 0.25, \text{ and } 0.50$ .

monotonically with the hybridization parameter  $V$  and reach a maximum at around  $V = 0.3$ . The nonmonotonic variation reflects the competition between in-plane phase coherence induced by the hybridization  $V$  and local interlayer pairing determined mainly by the superexchange  $J$ . We find  $T_c$  to be greatly reduced from bilayer to trilayer models. This observation is further supported by Fig. 1(d) where the trilayer  $T_c$  is plotted against  $J$  for three typical values of  $V = 0.15, 0.25, 0.50$ . We obtain the largest slope in the small  $J$  region, giving a maximum ratio  $T_c/J \approx 0.02 - 0.03$  for realistic parameters. While for the bilayer model, our previous calculations yield a maximum  $T_c/J \approx 0.04 - 0.05$  [44]. Interestingly, if we take heuristically the interlayer  $J$  to be 150 meV from RIXS measurements (assuming the spin size  $S \approx 1/2$ ) on  $\text{La}_3\text{Ni}_2\text{O}_7$  at ambient pressure [17], these ratios immediately predict a maximum  $T_c$  of about 70–90 K for the bilayer system and 30–50 K for the trilayer system, both consistent with experimental observations [1, 7]. By

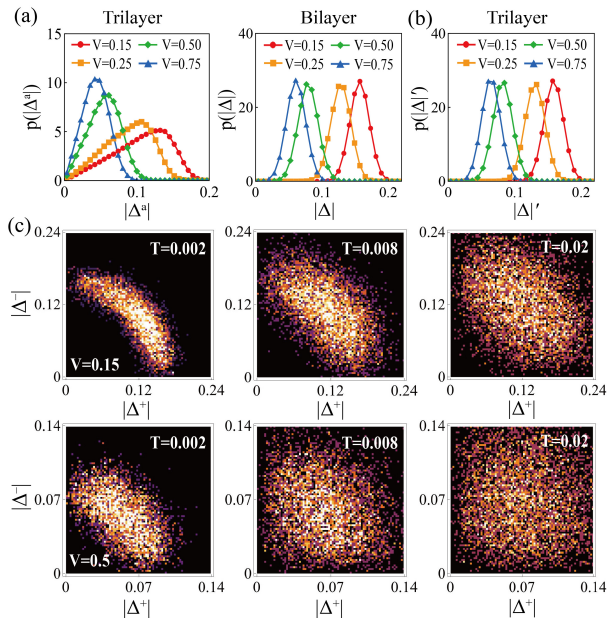


FIG. 2: (a) Comparison of the probability distributions of the pairing amplitudes  $p(|\Delta^a|)$  of the trilayer model (left) and  $p(|\Delta|)$  of the bilayer model (right) for different values of  $V = 0.15, 0.25, 0.50, 0.75$  at  $T = 0.002$ . (b) Probability distribution of the total pairing amplitude  $p(|\Delta'|)$  of the trilayer model, where  $|\Delta'| = \sqrt{|\Delta^+|^2 + |\Delta^-|^2}$ . (c) Intensity plot of the joint distribution of  $|\Delta^+|$  and  $|\Delta^-|$  of the trilayer model for  $V = 0.15, 0.5$  and  $T = 0.002, 0.008, 0.02$ , showing clear ring-shaped distribution at low temperatures and weak hybridizations. Other parameters are  $t_{\perp} = 0$  and  $J = 0.5$ .

contrast, the intralayer  $J$  is less than 10 meV at ambient pressure, while in cuprates, just oppositely, it is much larger than the interlayer one [101].

In reality, the magnitude of the trilayer  $T_c$  may be further reduced by other factors. First-principles calculations have revealed a subtle imbalance in  $\text{La}_4\text{Ni}_3\text{O}_{10}$ , with somewhat different hybridization  $V$  and chemical potential  $\mu$  between the inner and outer layers [66, 72]. Our calculations show that both tend to suppress  $T_c$  [93]. A small interlayer hopping may also influence  $T_c$  but acts similarly on both models. We therefore conclude that the reduction of  $T_c$  from bilayer to trilayer nickelates may be a genuine intrinsic property reflecting their interlayer pairing mechanism, different from the cuprates.

*Frustrated superconductivity.*—To clarify the origin of the  $T_c$  reduction, we present a comparative analysis of the probability distribution of the pairing field amplitudes in bilayer and trilayer models. As shown in Fig. 2(a), the trilayer  $p(|\Delta^a|)$  exhibits a broad peak extending almost linearly to  $|\Delta^a| = 0$ , in sharp contrast to that of the bilayer model. To understand this, we collect all Monte Carlo configurations of  $|\Delta^a|$  of the trilayer model on an intensity plot in Fig. 2(c) for two typical values

$V = 0.15$  and  $0.5$ . Quite unexpectedly, the data accumulate to form a ring shape at low temperatures. As the temperature increases, the ring gradually dissolves, resulting in nearly independent fluctuations of  $|\Delta^+|$  and  $|\Delta^-|$ . Note that the suppression of the distribution near horizontal and vertical axes is due to the phase space limitation of the amplitude. For small  $V = 0.15$ , the ring remains discernible even above  $T_c$  due to preformed pairs in this parameter region [102, 103].

The ring shape suggests some internal symmetry between  $|\Delta^{\pm}|$  and motivates us to define an overall pairing amplitude  $|\Delta'| \equiv \sqrt{|\Delta^+|^2 + |\Delta^-|^2}$ . Interestingly, as shown in Fig. 2(b), the trilayer  $p(|\Delta'|)$  exhibits almost identical distribution as the bilayer  $p(|\Delta|)$ . To see this more clearly, we plot in Fig. 1(c) the most probable value of  $|\Delta^a|$  and  $|\Delta'|$  of the trilayer model and  $|\Delta|$  of the bilayer model, and compare them with  $T_c$  after a common scaling. Surprisingly,  $|\Delta'|$  and  $|\Delta|$  fall upon the same curve and track exactly the  $T_c$  evolution of the bilayer model at large  $V$ , while  $|\Delta^a|$  is systematically smaller and falls upon the  $T_c$  curve of the trilayer model. Thus, the magnitudes of  $T_c$  in this region are determined by the pairing amplitudes in both models, and its reduction in the trilayer model must originate from the fluctuation between  $|\Delta^+|$  and  $|\Delta^-|$ . The superconductivity seems frustrated, where two outer layers compete to form the singlet with the inner layer to achieve an overall  $|\Delta'| \approx |\Delta|$ .

*Internal symmetry and Josephson coupling.*—To clarify the origin of the frustration, we expand the effective action up to fourth order by assuming uniform pairing fields for simplicity. This gives a Ginzburg-Landau (GL) free energy for the trilayer model:

$$f_{\text{GL}} = c_1 \Psi^\dagger \Psi + c_2 (\Psi^\dagger \Psi)^2 - 2h \mathcal{T}_x^\Delta, \quad (4)$$

where  $\Psi = (\Delta^+, \Delta^-)^T$  is a Higgs-like complex doublet order parameter,  $\mathcal{T}^\Delta = \frac{1}{2} \Psi^\dagger \boldsymbol{\sigma} \Psi$  is its pseudospin,  $c_{1/2}$  are two GL parameters determined by model details, and  $h \propto t_{\perp}^2$  plays the role of an effective transverse field [93].

We first consider  $t_{\perp} = 0$  since it is strongly renormalized and proportional to the density of self-doped holes on  $d_{z^2}$  ( $\delta_h \sim 0.01$ ). This gives  $h = 0$  and we immediately see that the GL free energy has a global  $\text{SU}(2) \times \text{U}(1)$  symmetry associated with the rotation of the pseudospin and an overall phase rotation. Both symmetries can be well understood from the original Hamiltonian (1), where the  $\text{SU}(2)$  corresponds to the basis transformation of  $(d_{+is}, d_{-is})^T$  and  $(c_{+is}, c_{-is})^T$  between two outer layers, and the  $\text{U}(1)$  reflects their phase change relative to the inner layer (charge conservation). For  $c_1 < 0$  and  $c_2 > 0$ ,  $\Psi^\dagger \Psi = |\Delta^+|^2 + |\Delta^-|^2$  acquires a nonzero expectation  $-c_1/2c_2$ , indicating a finite mean-field value of the total amplitude  $|\Delta'|$ . But the Mermin-Wagner theorem forbids spontaneous symmetry breaking at finite temperature, causing the ring-shaped joint distribution of  $|\Delta^+|$  and  $|\Delta^-|$  observed in Fig. 2(c). For the same reason, there

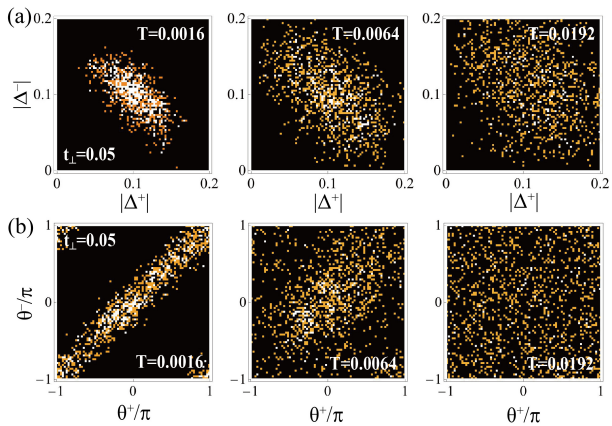


FIG. 3: Intensity plot of the joint distribution of (a) the pairing amplitudes  $|\Delta^\pm|$  and (b) their phases  $\theta^\pm$  of the trilayer model, showing strong fluctuations even deep inside the superconductivity for a finite  $t_\perp = 0.05$ . Other parameters are  $V = 0.15$  and  $J = 0.5$ , with  $T_c \approx 0.008$  reduced slightly from 0.009 at  $t_\perp = 0$ .

is no phase coherence between two superconducting layers, since  $\langle e^{-i(\theta^+ - \theta^-)} \rangle \propto \langle \bar{\Delta}^+ \Delta^- \rangle = \langle \mathcal{T}_x^\Delta \rangle + i \langle \mathcal{T}_y^\Delta \rangle = 0$ , which is also observed in our simulations. The free energy has the same form for the bilayer  $|\Delta|$ , explaining their almost identical distributions.

A nonzero interlayer hopping introduces a small but finite  $h \propto t_\perp^2 \propto \delta_h^2$ , which plays the role of a transverse field in the GL free energy and breaks the global  $SU(2)$  symmetry. For  $h > 0$  ( $< 0$ ), the GL free energy is minimized at  $\theta^+ = \theta^-$  ( $\theta^+ - \theta^- = \pi$ ) and  $|\Delta^+| = |\Delta^-|$ , with Gaussian fluctuations of both  $|\Delta^+| - |\Delta^-|$  and  $\theta^+ - \theta^-$  proportional to  $\delta_h^{-1}$  [93]. Thus, the fluctuations remain strong for small  $\delta_h$ . This is confirmed in Figs. 3(a) and 3(b) from our numerical calculations of the joint distribution of  $|\Delta^\pm|$  and  $\theta^\pm$  for  $t_\perp = 0.05$  and  $V = 0.15$ . Indeed, while the data get more clustered around the GL solution with lowering temperature, strong fluctuations persist even at  $T = 0.0016$  well below the BKT transition, indicating the lack of coherence along the  $c$ -axis. By rewriting  $\mathcal{T}_x^\Delta = |\Delta^+ \Delta^-| \cos(\theta^+ - \theta^-)$ , we see an intrinsic Josephson coupling within the trilayer structure, which predicts a Josephson frequency (if exist) only half that for intralayer pairing but is absent in the bilayer model [93]. We suggest future experiments to examine to what extent these features may be realized in real materials.

*Pairing symmetry.*—The mean-field gap structures in momentum space may be tentatively obtained by constructing a Bardeen-Cooper-Schrieffer (BCS) Hamiltonian with the static pairing fields  $\Delta^a$  and realistic tight-binding parameters [72]. First-principles calculations have predicted four Fermi pockets denoted as  $\alpha$ ,  $\beta_{1/2}$ , and  $\gamma$  in Fig. 4(a). Among them,  $\gamma$  comes mainly from the  $d_{z^2}$  bonding orbital, and all three others are hybridiza-

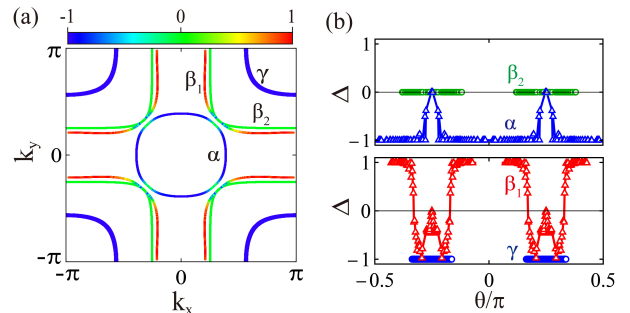


FIG. 4: (a) Illustration of some typical gap structures (normalized to their maximum values) on four Fermi pockets predicted by first-principles calculations. (b) Their variations with the azimuthal angle  $\theta$  within  $(-\pi/2, \pi/2)$ .

tion bands of both  $d_{z^2}$  and  $d_{x^2-y^2}$  characters. One may roughly think of the two outer layers to first form bonding and antibonding orbitals. Their antibonding orbitals give rise to the  $\beta_2$  Fermi surface, while their bonding orbitals further hybridize with the inner layer to form a bonding combination ( $\alpha$ ) and an antibonding combination ( $\beta_1$ ). Such bonding/antibonding characters determine most of their gap properties except for some narrow regions. The BCS Hamiltonian can be diagonalized to project out the gaps on each Fermi pocket. Figures 4(a) and 4(b) plot some typical results and we find extended  $s^\pm$ -wave gaps with (accidental) nodes along and close to the zone diagonal. Specifically, the gap on  $\gamma$  is nodeless, the gap on  $\alpha$  has the same sign as  $\gamma$  but contains nodes along the zone diagonal where the  $d_{x^2-y^2}$ - $d_{z^2}$  hybridization is zero, and the gap on  $\beta_1$  has an opposite sign on most regions of the Fermi surface with nodes along the zone diagonal but, depending on model details, may also change sign to give some accidental nodes near the zone diagonal. Notably,  $\beta_2$  remains metallic because of its antibonding character formed of two outer layers. Some of these details may change if other pairing channels are included. For example, introducing additional interlayer  $d_{x^2-y^2}$  pairing might eliminate the sign change and accidental nodes on  $\beta_1$ , while direct interlayer pairing of  $d_{z^2}$  between two outer layers would open a superconducting gap on  $\beta_2$ . But the main features, namely the extended  $s^\pm$ -wave pairing symmetry and the gap nodes (or minima) along the zone diagonal, are robust as long as the  $d_{z^2}$  interlayer pairing interaction dominates.

*Discussion and conclusions.*—We have proposed an interlayer pairing scenario for  $\text{La}_4\text{Ni}_3\text{O}_{10}$  and derived a reduced maximum ratio  $T_c/J \approx 0.02 - 0.03$  in the trilayer model from  $0.04 - 0.05$  in the bilayer model. We show that this reduction may be a natural consequence of interlayer pairing due to the competition of two outer layers to form spin-singlet pairs with the inner layer. This induces some kind of frustration and enhances the superconduct-

ing fluctuations between layers. Similar simulations for intralayer pairing have been performed for cuprates, but the maximum ratio  $T_c/J$  seems robust except for some very special situations [104]. It has been argued that the observed enhancement of maximum  $T_c$  in multilayer cuprates might actually come from the increase of the intralayer superexchange interaction or tuning to reach the optimal condition for maximizing  $T_c/J$ . While such details may be debated, our systematic comparison here reveals a probably fundamental distinction between two systems associated with their potentially different (interlayer vs intralayer) pairing mechanisms. An alternative explanation would be demanded if intralayer pairing governs bilayer and trilayer nickelate superconductors.

Lately, it has been reported that  $\text{La}_3\text{Ni}_2\text{O}_7$  may also adopt a single layer-trilayer alternate (1313) structure [105–107], raising the concerns regarding the true crystal structure responsible for its high-temperature superconductivity. While some recent experiments have already provided supportive evidences for the bilayer structure [108], our calculations here imply that the (1313) structure cannot give a maximum  $T_c$  as high as that in the bilayer structure.

This work was supported by the Strategic Priority Research Program of the Chinese Academy of Sciences (Grant No. XDB33010100), the National Natural Science Foundation of China (Grant No. 12174429), and the National Key Research and Development Program of China (Grant No. 2022YFA1402203).

Q.Q. and J.W. contributed equally to this work.

---

\* yifeng@iphy.ac.cn

- [1] H. Sun, M. Huo, X. Hu, J. Li, Z. Liu, Y. Han, L. Tang, Z. Mao, P. Yang, B. Wang, J. Cheng, D.-X. Yao, G.-M. Zhang, and M. Wang, Signatures of superconductivity near 80 K in a nickelate under high pressure, *Nature* **621**, 493 (2023).
- [2] J. Hou, P. T. Yang, Z. Y. Liu, J. Y. Li, P. F. Shan, L. Ma, G. Wang, N. N. Wang, H. Z. Guo, J. P. Sun, Y. Uwatoko, M. Wang, G.-M. Zhang, B. S. Wang, and J.-G. Cheng, Emergence of high-temperature superconducting phase in the pressurized  $\text{La}_3\text{Ni}_2\text{O}_7$  crystals, *Chin. Phys. Lett.* **40**, 117302 (2023).
- [3] Y. Zhang, D. Su, Y. Huang, Z. Shan, H. Sun, M. Huo, K. Ye, J. Zhang, Z. Yang, Y. Xu, Y. Su, R. Li, M. Smidman, M. Wang, L. Jiao, and H. Yuan, High-temperature superconductivity with zero-resistance and strange metal behavior in  $\text{La}_3\text{Ni}_2\text{O}_{7-\delta}$ , arXiv:2307.14819.
- [4] H. Sakakibara, M. Ochi, H. Nagata, Y. Ueki, H. Sakurai, R. Matsumoto, K. Terashima, K. Hirose, H. Ohta, M. Kato, Y. Takano, and K. Kuroki, Theoretical analysis on the possibility of superconductivity in the trilayer ruddlesden-popper nickelate  $\text{La}_4\text{Ni}_3\text{O}_{10}$  under pressure and its experimental examination: comparison with  $\text{La}_3\text{Ni}_2\text{O}_7$ , *Phys. Rev. B* **109**, 144511 (2024).
- [5] Q. Li, Y.-J. Zhang, Z.-N. Xiang, Y. Zhang, X. Zhu, and H.-H. Wen, Signature of superconductivity in pressurized  $\text{La}_4\text{Ni}_3\text{O}_{10}$ , *Chin. Phys. Lett.* **41**, 017401 (2024).
- [6] Y. Zhu, E. Zhang, B. Pan, X. Chen, D. Peng, L. Chen, H. Ren, F. Liu, N. Li, Z. Xing, J. Han, J. Wang, D. Jia, H. Wo, Y. Gu, Y. Gu, L. Ji, W. Wang, H. Gou, Y. Shen, T. Ying, X. Chen, W. Yang, C. Zheng, Q. Zeng, J. Guo, and J. Zhao, Superconductivity in trilayer nickelate  $\text{La}_4\text{Ni}_3\text{O}_{10}$  single crystals, arXiv:2311.07353.
- [7] M. Zhang, C. Pei, X. Du, W. Hu, Y. Cao, Q. Wang, J. Wu, Y. Li, H. Liu, C. Wen, Y. Zhao, C. Li, W. Cao, S. Zhu, Q. Zhang, N. Yu, P. Cheng, L. Zhang, Z. Li, J. Zhao, Y. Chen, H. Guo, C. Wu, F. Yang, S. Yan, L. Yang, and Y. Qi, Superconductivity in trilayer nickelate  $\text{La}_4\text{Ni}_3\text{O}_{10}$  under pressure, arXiv:2311.07423.
- [8] J. Li, C.-Q. Chen, C. Huang, Y. Han, M. Huo, X. Huang, P. Ma, Z. Qiu, J. Chen, X. Hu, L. Chen, T. Xie, B. Shen, H. Sun, D. Yao, and M. Wang, Structural transition, electric transport, and electronic structures in the compressed trilayer nickelate  $\text{La}_4\text{Ni}_3\text{O}_{10}$ , *SCPMA*, **67**, 117403 (2024).
- [9] Z. Liu, M. Huo, J. Li, Q. Li, Y. Liu, Y. Dai, X. Zhou, J. Hao, Y. Lu, M. Wang, and H.-H. Wen, Electronic correlations and partial gap in the bilayer nickelate  $\text{La}_3\text{Ni}_2\text{O}_7$ , arXiv:2307.02950.
- [10] J. Yang, H. Sun, X. Hu, Y. Xie, T. Miao, H. Luo, H. Chen, B. Liang, W. Zhu, G. Qu, C.-Q. Chen, M. Huo, Y. Huang, S. Zhang, F. Zhang, F. Yang, Z. Wang, Q. Peng, H. Mao, G. Liu, Z. Xu, T. Qian, D.-X. Yao, M. Wang, L. Zhao, and X. J. Zhou, Orbital-dependent electron correlation in double-layer nickelate  $\text{La}_3\text{Ni}_2\text{O}_7$ , arXiv:2309.01148.
- [11] G. Wang, N. N. Wang, X. L. Shen, J. Hou, L. Ma, L. F. Shi, Z. A. Ren, Y. D. Gu, H. M. Ma, P. T. Yang, Z. Y. Liu, H. Z. Guo, J. P. Sun, G. M. Zhang, S. Calder, J.-Q. Yan, B. S. Wang, Y. Uwatoko, and J.-G. Cheng, Pressure-Induced superconductivity in polycrystalline  $\text{La}_3\text{Ni}_2\text{O}_{7-\delta}$ , *Phys. Rev. X* **14**, 11040 (2024).
- [12] Y. Zhou, J. Guo, S. Cai, H. Sun, P. Wang, J. Zhao, J. Han, X. Chen, Y. Chen, Q. Wu, Y. Ding, T. Xiang, H. kwang Mao, and L. Sun, Evidence of filamentary superconductivity in pressurized  $\text{La}_3\text{Ni}_2\text{O}_7$ , arXiv:2311.12361.
- [13] T. Cui, S. Choi, T. Lin, C. Liu, G. Wang, N. Wang, S. Chen, H. Hong, D. Rong, Q. Wang, Q. Jin, J.-O. Wang, L. Gu, C. Ge, C. Wang, J. G. Cheng, Q. Zhang, L. Si, K. Juan Jin, and E.-J. Guo, Strain mediated phase crossover in ruddlesden popper nickelates, arXiv:2311.13228.
- [14] K. Chen, X. Liu, J. Jiao, M. Zou, Y. Luo, Q. Wu, N. Zhang, Y. Guo, and L. Shu, Evidence of spin density waves in  $\text{La}_3\text{Ni}_2\text{O}_{7-\delta}$ , arXiv:2311.15717.
- [15] Z. Dong, M. Huo, J. Li, J. Li, P. Li, H. Sun, Y. Lu, M. Wang, Y. Wang, and Z. Chen, Visualization of oxygen vacancies and self-doped ligand holes in  $\text{La}_3\text{Ni}_2\text{O}_{7-\delta}$ , arXiv:2312.15727 (2023).
- [16] T. Xie, M. Huo, X. Ni, F. Shen, X. Huang, H. Sun, H. C. Walker, D. Adroja, D. Yu, B. Shen, L. He, K. Cao, and M. Wang, Neutron scattering studies on the high- $T_c$  superconductor  $\text{La}_3\text{Ni}_2\text{O}_{7-\delta}$  at ambient pressure, arXiv:2401.12635.
- [17] X. Chen, J. Choi, Z. Jiang, J. Mei, K. Jiang, J. Li, S. Agrestini, M. Garcia-Fernandez, X. Huang, H. Sun, D. Shen, M. Wang, J. Hu, Y. Lu, K.-J. Zhou, and D.

- Feng, Electronic and magnetic excitations in  $\text{La}_3\text{Ni}_2\text{O}_7$ , arXiv:2401.12657.
- [18] Z. Dan, Y. Zhou, M. Huo, Y. Wang, L. Nie, M. Wang, T. Wu, and X. Chen, Spin-density-wave transition in double-layer nickelate  $\text{La}_3\text{Ni}_2\text{O}_7$ , arXiv:2402.03952.
- [19] S. N. Abadi, K. Xu, E. G. Lomeli, P. Puphal, M. Isobe, Y. Zhong, A. V. Fedorov, S. Mo, M. Hashimoto, D. Lu, B. Moritz, B. Keimer, T. P. Devereaux, M. Hepting, and Zhi-Xun Shen, Electronic structure of the alternating monolayer-trilayer phase of  $\text{La}_3\text{Ni}_2\text{O}_7$ , arXiv:2402.07143.
- [20] N. Yuan, A. Elghandour, J. Arneth, K. Dey, and R. Klingeler, High-pressure crystal growth and investigation of the metal-to-metal transition of ruddlesden-popper trilayer nickelates  $\text{La}_4\text{Ni}_3\text{O}_{10}$ , Journal of Crystal Growth **627**, 127511 (2024).
- [21] M. Kakoi, T. Oi, Y. Ohshita, M. Yashima, K. Kuroki, T. Kato, H. Takahashi, S. Ishiwata, Y. Adachi, N. Hatada, T. Uda, and H. Mukuda, Multiband metallic ground state in multilayered nickelates  $\text{La}_3\text{Ni}_2\text{O}_7$  and  $\text{La}_4\text{Ni}_3\text{O}_{10}$  Probed by  $^{139}\text{La}$ -NMR at Ambient Pressure, arXiv:2312.11844.
- [22] Z. Luo, X. Hu, M. Wang, W. Wú, and D.-X. Yao, Bilayer two-orbital model of  $\text{La}_3\text{Ni}_2\text{O}_7$  under pressure, Phys. Rev. Lett. **131**, 126001 (2023).
- [23] Y. Zhang, L.-F. Lin, A. Moreo, and E. Dagotto, Electronic structure, dimer physics, orbital-selective behavior, and magnetic tendencies in the bilayer nickelate superconductor  $\text{La}_3\text{Ni}_2\text{O}_7$  under pressure, Phys. Rev. B **108**, L180510 (2023).
- [24] Q.-G. Yang, D. Wang, and Q.-H. Wang, Possible  $s_{\pm}$ -wave superconductivity in  $\text{La}_3\text{Ni}_2\text{O}_7$ , Phys. Rev. B **108**, L140505 (2023).
- [25] F. Lechermann, J. Gondolf, S. Bötzel, and I. M. Eremin, Electronic correlations and superconducting instability in  $\text{La}_3\text{Ni}_2\text{O}_7$  under high pressure, Phys. Rev. B **108**, L201121 (2023).
- [26] H. Sakakibara, N. Kitamine, M. Ochi, and K. Kuroki, Possible high  $T_c$  superconductivity in  $\text{La}_3\text{Ni}_2\text{O}_7$  under high pressure through manifestation of a nearly-half-filled bilayer Hubbard model, Phys. Rev. Lett. **132**, 106002 (2024).
- [27] Y. Gu, C. Le, Z. Yang, X. Wu, and J. Hu, Effective model and pairing tendency in bilayer Ni-based superconductor  $\text{La}_3\text{Ni}_2\text{O}_7$ , arXiv:2306.07275.
- [28] Y. Shen, M. Qin, and G.-M. Zhang, Effective bilayer model hamiltonian and density-matrix renormalization group study for the high- $T_c$  superconductivity in  $\text{La}_3\text{Ni}_2\text{O}_7$  under high pressure, Chin. Phys. Lett. **40**, 127401 (2023).
- [29] V. Christiansson, F. Petocchi, and P. Werner, Correlated electronic structure of  $\text{La}_3\text{Ni}_2\text{O}_7$  under pressure, Phys. Rev. Lett. **131**, 206501 (2023).
- [30] D. A. Shilenko and I. V. Leonov, Correlated electronic structure, orbital-selective behavior, and magnetic correlations in double-layer  $\text{La}_3\text{Ni}_2\text{O}_7$  under pressure, Phys. Rev. B **108**, 125105 (2023).
- [31] W. Wú, Z. Luo, D.-X. Yao, and M. Wang, Charge transfer and Zhang-Rice singlet bands in the nickelate superconductor  $\text{La}_3\text{Ni}_2\text{O}_7$  under pressure, arXiv:2307.05662.
- [32] Y. Cao and Y.-F. Yang, Flat bands promoted by Hund's rule coupling in the candidate double-layer high-temperature superconductor  $\text{La}_3\text{Ni}_2\text{O}_7$ , Phys. Rev. B **109**, L081105 (2024).
- [33] X. Chen, P. Jiang, J. Li, Z. Zhong, and Y. Lu, Critical charge and spin instabilities in superconducting  $\text{La}_3\text{Ni}_2\text{O}_7$ , arXiv:2307.07154.
- [34] Y.-B. Liu, J.-W. Mei, F. Ye, W.-Q. Chen, and F. Yang,  $s^{\pm}$ -Wave pairing and the destructive role of apical-oxygen deficiencies in  $\text{La}_3\text{Ni}_2\text{O}_7$  under pressure, Phys. Rev. Lett. **131**, 236002 (2023).
- [35] C. Lu, Z. Pan, F. Yang, and C. Wu, Interlayer coupling driven high-temperature superconductivity in  $\text{La}_3\text{Ni}_2\text{O}_7$  under pressure, Phys. Rev. Lett. **132**, 146002 (2024).
- [36] Y. Zhang, L.-F. Lin, A. Moreo, T. A. Maier, and E. Dagotto, Structural phase transition,  $s_{\pm}$ -wave pairing and magnetic stripe order in the bilayered nickelate superconductor  $\text{La}_3\text{Ni}_2\text{O}_7$  under pressure, Nat. Commun. **15**, 2470 (2024).
- [37] H. Oh and Y.-H. Zhang, Type-II  $t$ - $J$  model and shared superexchange coupling from Hund's rule in superconducting  $\text{La}_3\text{Ni}_2\text{O}_7$ , Phys. Rev. B **108**, 174511 (2023).
- [38] Z. Liao, L. Chen, G. Duan, Y. Wang, C. Liu, R. Yu, and Q. Si, Electron correlations and superconductivity in  $\text{La}_3\text{Ni}_2\text{O}_7$  under pressure tuning, Phys. Rev. B **108**, 214522 (2023).
- [39] X.-Z. Qu, D.-W. Qu, J. Chen, C. Wu, F. Yang, W. Li, and G. Su, Bilayer  $t$ - $J$ - $J_{\perp}$  model and magnetically mediated pairing in the pressurized nickelate  $\text{La}_3\text{Ni}_2\text{O}_7$ , Phys. Rev. Lett. **132**, 036502 (2024).
- [40] Y.-F. Yang, G.-M. Zhang, and F.-C. Zhang, Interlayer valence bonds and two-component theory for high- $T_c$  superconductivity of  $\text{La}_3\text{Ni}_2\text{O}_7$  under pressure, Phys. Rev. B **108**, L201108 (2023).
- [41] K. Jiang, Z. Wang, and F.-C. Zhang, High-temperature superconductivity in  $\text{La}_3\text{Ni}_2\text{O}_7$ , Chin. Phys. Lett. **41**, 017402 (2024).
- [42] Y. Zhang, L.-F. Lin, A. Moreo, T. A. Maier, and E. Dagotto, Trends in electronic structures and  $s_{\pm}$ -wave pairing for the rare-earth series in bilayer nickelate superconductor  $R_3\text{Ni}_2\text{O}_7$ , Phys. Rev. B **108**, 165141 (2023).
- [43] J. Huang, Z. D. Wang, and T. Zhou, Impurity and vortex states in the bilayer high-temperature superconductor  $\text{La}_3\text{Ni}_2\text{O}_7$ , Phys. Rev. B **108**, 174501 (2023).
- [44] Q. Qin and Y.-F. Yang, High- $T_c$  superconductivity by mobilizing local spin singlets and possible route to higher  $T_c$  in pressurized  $\text{La}_3\text{Ni}_2\text{O}_7$ , Phys. Rev. B **108**, L140504 (2023).
- [45] Y.-H. Tian, Y. Chen, J.-M. Wang, R.-Q. He, and Z.-Y. Lu, Correlation effects and concomitant two-orbital  $s_{\pm}$ -wave superconductivity in  $\text{La}_3\text{Ni}_2\text{O}_7$  under high pressure, Phys. Rev. B **109**, 165154 (2024).
- [46] Z. Luo, B. Lv, M. Wang, W. Wú, and D.-X. Yao, High  $T_c$  superconductivity in  $\text{La}_3\text{Ni}_2\text{O}_7$  based on the bilayer two-orbital  $t$ - $J$  model, arXiv:2308.16564.
- [47] J.-X. Zhang, H.-K. Zhang, Y.-Z. You, and Z.-Y. Weng, Strong pairing originated from an emergent  $\mathbb{Z}_2$  Berry phase in  $\text{La}_3\text{Ni}_2\text{O}_7$ , arXiv:2309.05726.
- [48] B. Geisler, J. J. Hamlin, G. R. Stewart, R. G. Hennig, and P. J. Hirschfeld, Structural transitions, octahedral rotations, and electronic properties of  $A_3\text{Ni}_2\text{O}_7$  rare-earth nickelates under high pressure, npj Quantum Mater. **9**, 38 (2024).
- [49] T. Kaneko, H. Sakakibara, M. Ochi, and K. Kuroki, Pair correlations in the two-orbital Hubbard ladder: Implications for superconductivity in the bilayer nickelate  $\text{La}_3\text{Ni}_2\text{O}_7$ , Phys. Rev. B **109**, 045154 (2024).

- [50] C. Lu, Z. Pan, F. Yang, and C. Wu, Interplay of two  $E_g$  orbitals in superconducting  $\text{La}_3\text{Ni}_2\text{O}_7$  under pressure, arXiv:2310.02915.
- [51] S. Ryee, N. Witt, and T. O. Wehling, Quenched pair breaking by interlayer correlations as a key to superconductivity  $\text{La}_3\text{Ni}_2\text{O}_7$ , arXiv:2310.17465.
- [52] J. Chen, F. Yang, and W. Li, Orbital-selective superconductivity in the pressurized bilayer nickelate  $\text{La}_3\text{Ni}_2\text{O}_7$ : An infinite projected entangled-pair state study, arXiv:2311.05491.
- [53] H. Liu, C. Xia, S. Zhou, and H. Chen, Role of crystal-field-splitting and long-range-hoppings on superconducting pairing symmetry of  $\text{La}_3\text{Ni}_2\text{O}_7$ , arXiv:2311.07316.
- [54] L. Wang, Y. Li, S. Xie, F. Liu, H. Sun, C. Huang, Y. Gao, T. Nakagawa, B. Fu, B. Dong, Z. Cao, R. Yu, S. I.Kawaguchi, H. Kadobayashi, M. Wang, C. Jin, H. kwangMao, and H. Liu, Structure responsible for the superconducting state in  $\text{La}_3\text{Ni}_2\text{O}_7$  at high pressure and low temperature conditions, arXiv:2311.09186.
- [55] W.-X. Chang, S. Guo, Y.-Z. You, and Z.-X. Li, Fermi surface symmetric mass generation: a quantum Monte-Carlo study, arXiv:2311.09970.
- [56] Z. Ouyang, J.-M. Wang, J.-X. Wang, R.-Q. He, L. Huang, and Z.-Y. Lu, Hund electronic correlation in  $\text{La}_3\text{Ni}_2\text{O}_7$  under high pressure, *Phys. Rev. B* **109**, 115114 (2024).
- [57] X.-Z. Qu, D.-W. Qu, W. Li, and G. Su, Roles of Hund's rule and hybridization in the two-orbital model for high- $T_c$  superconductivity in the bilayer nickelate, arXiv:2311.12769.
- [58] Y.-Y. Zheng and W. Wú, Superconductivity in the bilayer two-orbital Hubbard model, arXiv:2312.03605.
- [59] G. Heier, K. Park, and S. Y. Savrasov, Competing  $d_{xy}$  and  $s_{\pm}$  pairing symmetries in superconducting  $\text{La}_3\text{Ni}_2\text{O}_7$  emerge from LDA+FLEX calculations, arXiv:2312.04401.
- [60] Z. Fan, J.-F. Zhang, B. Zhan, D. Lv, X.-Y. Jiang, B. Normand, and T. Xiang, Superconductivity in nickelate and cuprate superconductors with strong bilayer coupling, arXiv:2312.17064.
- [61] E. F. Talantsev and V. V. Chistyakov, Debye temperature, electron-phonon coupling constant, and microcrystalline strain in highly-compressed  $\text{La}_3\text{Ni}_2\text{O}_{7-\delta}$ , arXiv:2401.00804.
- [62] Y. Wang, K. Jiang, Z. Wang, F.-C. Zhang, and J. Hu, Electronic structure and superconductivity in bilayer  $\text{La}_3\text{Ni}_2\text{O}_7$ , arXiv:2401.15097.
- [63] S. Botzel, F. Lechermann, J. Gondolf, and I. M. Eremin, Theory of magnetic excitations in multilayer nickelate superconductor  $\text{La}_3\text{Ni}_2\text{O}_7$ , arXiv:2401.16151.
- [64] J.-R. Xue and F. Wang, Magnetism and superconductivity in the  $t$ - $J$  model of  $\text{La}_3\text{Ni}_2\text{O}_7$  under multiband gutzwiller approximation, arXiv:2402.07449 (2024).
- [65] I. V. Leonov, Electronic structure and magnetic correlations in trilayer nickelate superconductor  $\text{La}_4\text{Ni}_3\text{O}_{10}$  under pressure, arXiv:2401.07350.
- [66] P.-F. Tian, H.-T. Ma, X. Ming, X.-J. Zheng, and H. Li, Effective model and electron correlations in trilayer nickelate superconductor  $\text{La}_4\text{Ni}_3\text{O}_{10}$ , arXiv:2402.02351.
- [67] J.-X. Wang, Z. Ouyang, R.-Q. He, and Z.-Y. Lu, Non-Fermi liquid and hund correlation in  $\text{La}_4\text{Ni}_3\text{O}_{10}$  under high pressure, *Phys. Rev. B* **109**, 165140 (2024).
- [68] H. LaBollita, J. Kapeghian, M. R. Norman, and A. S.Botana, Electronic structure and magnetic tendencies of trilayer  $\text{La}_4\text{Ni}_3\text{O}_{10}$  under pressure: structural transition, molecular orbitals, and layer differentiation, arXiv:2402.05085.
- [69] Y. Zhang, L.-F. Lin, A. Moreo, T. A. Maier, and E. Dagotto, Prediction of  $s_{\pm}$ -wave superconductivity enhanced by electronic doping in trilayer nickelates  $\text{La}_4\text{Ni}_3\text{O}_{10}$  under pressure, arXiv:2402.05285.
- [70] Q.-G. Yang, K.-Y. Jiang, D. Wang, H.-Y. Lu, and Q.-H. Wang, Effective model and  $s_{\pm}$ -wave superconductivity in trilayer nickelate  $\text{La}_4\text{Ni}_3\text{O}_{10}$ , arXiv:2402.05447.
- [71] C. Lu, Z. Pan, F. Yang, and C. Wu, Superconductivity in  $\text{La}_4\text{Ni}_3\text{O}_{10}$  under pressure, arXiv:2402.06450.
- [72] C.-Q. Chen, Z. Luo, M. Wang, W. Wú, and D.-X. Yao, Trilayer multi-orbital models of  $\text{La}_4\text{Ni}_3\text{O}_{10}$ , arXiv:2402.07196.
- [73] M. Zhang, H. Sun, Y.-B. Liu, Q. Liu, W.-Q. Chen, and F. Yang, The  $s_{\pm}$ -wave superconductivity in the pressurized  $\text{La}_4\text{Ni}_3\text{O}_{10}$ , arXiv:2402.07902.
- [74] D. J. Scalapino, A common thread: The pairing interaction for unconventional superconductors. *Rev. Mod. Phys.* **84**, 1383 (2012).
- [75] Z. Wang, C. Zou, C. Lin, X. Luo, H. Yan, C. Yin, Y. Xu, X. Zhou, Y. Wang, and J. Zhu, Correlating the charge-transfer gap to the maximum transition temperature in  $\text{Bi}_2\text{Sr}_2\text{Ca}_{n-1}\text{Cu}_n\text{O}_{2n+4\delta}$ , *Science* **381**, 227 (2023).
- [76] H. Li, X. Zhou, T. Nummy, J. Zhang, V. Pardo, W. E.Pickett, J. F. Mitchell, and D. S. Dessau, Fermiology and electron dynamics of trilayer nickelate  $\text{La}_4\text{Ni}_3\text{O}_{10}$ , *Nat. Commun.* **8**, 704 (2017).
- [77] M. Mayr, G. Alvarez, C. Şen, and E. Dagotto, Phase fluctuations in strongly coupled  $d$ -wave superconductors, *Phys. Rev. Lett.* **94**, 217001 (2005).
- [78] Y. Dubi, Y. Meir, and Y. Avishai, Nature of the superconductor-insulator transition in disordered superconductors, *Nature* **449**, 876 (2007).
- [79] M. Karmakar, Pauli limited  $d$ -wave superconductors: quantum breached pair phase and thermal transitions, *J. Phys. Condens. Matter* **32**, 405604 (2020).
- [80] K. Pasrija, P. B. Chakraborty, and S. Kumar, Effective Hamiltonian based Monte Carlo for the BCS to BEC crossover in the attractive Hubbard model, *Phys. Rev. B* **94**, 165150 (2016).
- [81] J.-J. Dong, D. Huang, and Y.-F. Yang, Mutual information, quantum phase transition, and phase coherence in Kondo systems, *Phys. Rev. B* **104**, L081115 (2021).
- [82] J.-J. Dong and Y.-F. Yang, Development of long-range phase coherence on the Kondo lattice, *Phys. Rev. B* **106**, L161114 (2022).
- [83] A. Mukherjee, N. D. Patel, S. Dong, S. Johnston, A. Moreo, and E. Dagotto, Testing the Monte Carlo-mean field approximation in the one-band Hubbard model, *Phys. Rev. B* **90**, 205113 (2014).
- [84] S. Liang, A. Moreo, and E. Dagotto, Nematic state of pnictides stabilized by interplay between spin, orbital, and lattice degrees of freedom, *Phys. Rev. Lett.* **111**, 047004 (2013).
- [85] Q. Qin, J.-J. Dong, Y. Sheng, D. Huang, and Y.-F. Yang, Superconducting fluctuations and charge- $4e$  plaquette state at strong coupling, *Phys. Rev. B* **108**, 054506 (2023).
- [86] Q. Han, T. Li, and Z. D. Wang, Pseudogap and Fermi-arc evolution in the phase-fluctuation scenario, *Phys. Rev. B* **82**, 052503 (2010).

- [87] Y. W. Zhong, T. Li, and Q. Han, Monte Carlo Study of thermal fluctuations and Fermi-arc formation in  $d$ -wave superconductors, *Phys. Rev. B* **84**, 024522 (2011).
- [88] D. K. Singh, S. Kadge, Y. Bang, and P. Majumdar, Fermi arcs and pseudogap phase in a minimal microscopic model of  $d$ -wave superconductivity, *Phys. Rev. B* **105**, 054501 (2022).
- [89] P. Coleman, *Introduction to Many-body Physics*, (Cambridge University Press, Cambridge, U.K., 2015).
- [90] V. L. Berezinskii, Destruction of long-range order in one-dimensional and two-dimensional systems possessing a continuous symmetry group. II. Quantum Systems, *Zh. Eksp. Teor. Fiz.* **61**, 1144 (1971) [*Sov. Phys. JETP* **34**, 610 (1972)].
- [91] J. M. Kosterlitz and D. J. Thouless, Ordering, metastability and phase transitions in two-dimensional systems, *J. Phys. C* **6**, 1181 (1973).
- [92] J. M. Kosterlitz, The critical properties of the two-dimensional XY model, *J. Phys. C* **7**, 1046 (1974).
- [93] See Supplemental Material for more details on the derivation of the effective action, the Ginzburg-Landau free energy, the Josephson effect, and the influence of the layer imbalance on  $T_c$ .
- [94] V. Drouin-Touchette, The Kosterlitz-Thouless phase transition: an introduction for the intrepid student, arXiv:2207.13748.
- [95] T. M. Cover and J. A. Thomas, *Elements of Information Theory*, Wiley Series in Telecommunications and Signal Processing (Wiley-Interscience, Hoboken, NJ, 2006).
- [96] A. Kraskov, H. Stögbauer, and P. Grassberger, Estimating mutual information, *Phys. Rev. E* **69**, 066138 (2004).
- [97] G. A. Darbellay and I. Vajda, Estimation of the information by an adaptive partitioning of the observation space, *IEEE Trans. Inf. Theory* **45**, 1315 (1999).
- [98] S. Khan, S. Bandyopadhyay, A. R. Ganguly, S. Saigal, D. J. Erickson, V. Protopopescu, and G. Ostrouchov, Relative performance of mutual information estimation methods for quantifying the dependence among short and noisy data, *Phys. Rev. E* **76**, 026209 (2007).
- [99] M. I. Belghazi, A. Baratin, S. Rajeswar, S. Ozair, Y. Bengio, A. Courville, and R. D. Hjelm, Mutual information neural estimation, in *Proceedings of the 35th International Conference on Machine Learning, Stockholmsmässan, Stockholm Sweden*, edited by J. Dy and A. Krause (PMLR, Stockholmsmässan, Stockholm Sweden, 2018), p. 531.
- [100] B. Poole, S. Ozair, A. V. D. Oord, A. A. Alemi, and G. Tucker, On variational bounds of mutual information, in *Proceedings of the 36th International Conference on Machine Learning, Long Beach, California, USA*, edited by K. Chaudhuri and R. Salakhutdinov (PMLR, Long Beach, California, USA, 2019), p. 5171.
- [101] M. Le Tacon, G. Ghiringhelli, J. Chaloupka, M. M. Sala, V. Hinkov, M. W. Haverkort, M. Minola, M. Bakr, K. J. Zhou, S. Blanco-Canosa, C. Monney, Y. T. Song, G. L. Sun, C. T. Lin, G. M. De Luca, M. Salluzzo, G. Khal-iullin, T. Schmitt, L. Braicovich, and B. Keimer, Intense paramagnon excitations in a large family of high-temperature superconductors, *Nat. Phys.* **7**, 725 (2011).
- [102] B. Keimer, S. A. Kivelson, M. R. Norman, S. Uchida, and J. Zaanen, From quantum matter to high-temperature superconductivity in copper oxides, *Nature* **518**, 179 (2015).
- [103] V. J. Emery and S. A. Kivelson, Importance of phase fluctuations in superconductors with small superfluid density, *Nature* **374**, 434 (1995).
- [104] Q. Qin and Y.-F. Yang, Intrinsic constraint on  $T_c$  for unconventional superconductivity, arXiv:2402.07128.
- [105] X. Chen, J. Zhang, A. S. Thind, S. Sharma, H. LaBollita, G. Peterson, H. Zheng, D. Phelan, A. S. Botana, R. F. Klie, and J. F. Mitchell, Polymorphism in ruddlesden-popper  $\text{La}_3\text{Ni}_2\text{O}_7$ : Discovery of a hidden phase with distinctive layer stacking, arXiv:2312.06081.
- [106] P. Puphal, P. Reiss, N. Enderlein, Y.-M. Wu, G. Khal-iullin, V. Sundaramurthy, T. Priessnitz, M. Knauff, L. Richter, M. Isobe, P. A. van Aken, H. Takagi, B. Keimer, Y. E. Suyolcu, B. Wehinger, P. Hansmann, and M. Hepting, Unconventional crystal structure of the high-pressure superconductor  $\text{La}_3\text{Ni}_2\text{O}_7$ , arXiv:2312.07341.
- [107] H. Wang, L. Chen, A. Rutherford, H. Zhou, and W. Xie, Long-range structural order in a hidden phase of ruddlesden-popper bilayer nickelates  $\text{La}_3\text{Ni}_2\text{O}_7$ , *Inorg. Chem.* **63**, 5020 (2024).
- [108] J. Li, P. Ma, H. Zhang, X. Huang, C. Huang, M. Huo, D. Hu, Z. Dong, C. He, J. Liao, X. Chen, T. Xie, H. Sun, and M. Wang, Pressure-driven right-triangle shape superconductivity in bilayer nickelate  $\text{La}_3\text{Ni}_2\text{O}_7$ , arXiv:2404.11369.

# Frustrated Superconductivity in the Trilayer Nickelate $\text{La}_4\text{Ni}_3\text{O}_{10}$

## - Supplemental Material -

Qiong Qin,<sup>1,2</sup> Jiangfan Wang,<sup>3</sup> and Yi-feng Yang<sup>1,2,4,\*</sup>

<sup>1</sup>*Beijing National Laboratory for Condensed Matter Physics and Institute of Physics,  
Chinese Academy of Sciences, Beijing 100190, China*

<sup>2</sup>*University of Chinese Academy of Sciences, Beijing 100049, China*

<sup>3</sup>*School of Physics, Hangzhou Normal University, Hangzhou, Zhejiang 311121, China*

<sup>4</sup>*Songshan Lake Materials Laboratory, Dongguan, Guangdong 523808, China*

### A. Derivation of the effective action

We use the coherent-state path integral to transform the Hamiltonian to the following action:

$$S = \int_0^\beta d\tau \left\{ \sum_{lij_s} \bar{c}_{lis}(\tau) [(\partial_\tau - \mu)\delta_{ij} - t_{ij}] c_{ljs}(\tau) + \sum_{lis} \bar{d}_{lis}(\tau) \partial_\tau d_{lis}(\tau) - \sum_{lij_s} V_{ij} (\bar{d}_{lis}(\tau) c_{ljs}(\tau) + c.c.) - t_\perp \sum_{ais} (\bar{d}_{ois}(\tau) d_{ais}(\tau) + c.c.) - \frac{3J}{4} \sum_{ai} \bar{\Phi}_i^a(\tau) \Phi_i^a(\tau) \right\}. \quad (\text{S1})$$

where  $\Phi_i^a(\tau) = \frac{1}{\sqrt{2}} [d_{0i\downarrow}(\tau) d_{ai\uparrow}(\tau) - d_{0i\uparrow}(\tau) d_{ai\downarrow}(\tau)]$  denotes the local interlayer spin-singlet pairing of  $d_{z^2}$  at site  $i$  between the inner layer and the  $a$ -th outer layer.

The auxiliary interlayer pairing fields  $\Delta_i^a(\tau)$  are then introduced to decouple the pairing term:

$$-\frac{3J}{4} \bar{\Phi}_i^a(\tau) \Phi_i^a(\tau) \rightarrow \sqrt{2} \bar{\Delta}_i^a(\tau) \Phi_i^a(\tau) + \sqrt{2} \bar{\Phi}_i^a(\tau) \Delta_i^a(\tau) + \frac{8\bar{\Delta}_i^a(\tau) \Delta_i^a(\tau)}{3J}, \quad (\text{S2})$$

where  $\bar{\Delta}_i^a(\tau)$  is the complex conjugate of  $\Delta_i^a(\tau)$ . In the static auxiliary field approximation, we ignore the imaginary time dependence of the auxiliary fields,  $\Delta_i^a(\tau) \rightarrow \Delta_i^a$ , but retain their spatial dependence.

Upon Fourier transformation, the above action becomes

$$S = \sum_n \bar{\psi}_n(-i\omega_n + O) \psi_n + \frac{8\beta}{3J} \sum_{ia} |\Delta_i^a|^2, \quad (\text{S3})$$

where  $\bar{\psi}_n = (\bar{c}_{+\uparrow}, c_{0\downarrow}, \bar{c}_{-\uparrow}, c_{+\downarrow}, \bar{c}_{0\uparrow}, c_{-\downarrow}, \bar{d}_{+\uparrow}, d_{0\downarrow}, \bar{d}_{-\uparrow}, d_{+\downarrow}, \bar{d}_{0\uparrow}, d_{-\downarrow})$  in which  $\bar{c}_{ls}$  and  $\bar{d}_{ls}$  are both row vectors of length  $N$  (the lattice size) denoting  $(\bar{c}_{l1s}(\tilde{s}i\omega_n), \dots, \bar{c}_{lNs}(\tilde{s}i\omega_n))$  and  $(\bar{d}_{l1s}(\tilde{s}i\omega_n), \dots, \bar{d}_{lNs}(\tilde{s}i\omega_n))$ , respectively. Here  $\tilde{s} = 1$  for  $s = \uparrow$  and  $\tilde{s} = -1$  for  $s = \downarrow$ . The matrix  $O$  takes the form:

$$O = \begin{pmatrix} A_1 & B_1 \\ B_1 & D_1 \end{pmatrix}, \quad A_1 = \begin{pmatrix} A & 0 \\ 0 & -A \end{pmatrix}, \quad B_1 = \begin{pmatrix} B & 0 \\ 0 & -B \end{pmatrix}, \quad D_1 = \begin{pmatrix} M & D \\ -D & M^* \end{pmatrix}, \quad (\text{S4})$$

with

$$A = \begin{pmatrix} -T & 0 & 0 \\ 0 & T & 0 \\ 0 & 0 & -T \end{pmatrix}, \quad B = \begin{pmatrix} -\mathcal{V} & 0 & 0 \\ 0 & \mathcal{V} & 0 \\ 0 & 0 & -\mathcal{V} \end{pmatrix}, \quad D = \begin{pmatrix} 0 & -T_\perp & 0 \\ T_\perp & 0 & T_\perp \\ 0 & -T_\perp & 0 \end{pmatrix}, \quad M = \begin{pmatrix} 0 & M_+ & 0 \\ M_+^* & 0 & M_-^* \\ 0 & M_- & 0 \end{pmatrix}, \quad (\text{S5})$$

where  $T_{ij} = t_{ij} + \mu\delta_{ij}$ ,  $(T_\perp)_{ij} = t_\perp\delta_{ij}$ ,  $\mathcal{V}_{ij} = V_{ij}$ , and  $(M_a)_{ij} = \Delta_i^a\delta_{ij}$  with  $i, j = 1, \dots, N$ .

For numerical simulations, we integrate out the fermionic degrees of freedom and obtain the effective action of the auxiliary pairing fields:

$$S_{\text{eff}}(\{\Delta_i^a\}) = \frac{8\beta}{3J} \sum_{ia} \bar{\Delta}_i^a \Delta_i^a - \sum_i \ln(1 + e^{-\beta\tilde{\Lambda}_i}) - \sum_i \ln(1 + e^{-\beta\Lambda_i}), \quad (\text{S6})$$

where  $\tilde{\Lambda}_i$  and  $\Lambda_i$  are the eigenvalues of the matrix  $A_1$  and  $Q = B_1 A_1^{-1} B_1 + D_1$  to reduce the computational time. This is exactly Eq. (3) in the main text.

When  $t_{\perp} = 0$ ,  $D_1$  is diagonal and the above procedure can be further simplified to give

$$S = \sum_n \bar{\psi}_{1n}(-i\omega_n + O_1)\psi_{1n} + \sum_n \bar{\psi}_{2n}(-i\omega_n + O_2)\psi_{2n} + \frac{8\beta}{3J} \sum_{ia} |\Delta_i^a|^2, \quad (\text{S7})$$

where

$$\bar{\psi}_{1n} = (\bar{c}_{+\uparrow}(i\omega_n), c_{0\downarrow}(-i\omega_n), \bar{c}_{-\uparrow}(i\omega_n), \bar{d}_{+\uparrow}(i\omega_n), d_{0\downarrow}(-i\omega_n), \bar{d}_{-\uparrow}(i\omega_n)), \quad (\text{S8})$$

$$\bar{\psi}_{2n} = (c_{+\downarrow}(-i\omega_n), \bar{c}_{0\uparrow}(i\omega_n), c_{-\downarrow}(-i\omega_n), d_{+\downarrow}(-i\omega_n), \bar{d}_{0\uparrow}(i\omega_n), d_{-\downarrow}(-i\omega_n)). \quad (\text{S9})$$

Again,  $\bar{c}_{ls}(i\omega_n)$  and  $\bar{d}_{ls}(i\omega_n)$  are row vectors of length  $N$  as defined above. The matrices  $O_1$  and  $O_2$  are:

$$O_1 = \begin{pmatrix} A & B \\ B & M \end{pmatrix}, \quad O_2 = \begin{pmatrix} -A & -B \\ -B & M^* \end{pmatrix}. \quad (\text{S10})$$

Integrating out the fermionic degrees of freedom gives the effective action:

$$S_{\text{eff}}(\{\Delta_i^a\}) = \frac{8\beta}{3J} \sum_{ia} \bar{\Delta}_i^a \Delta_i^a - \sum_{i;s=\pm} \ln(1 + e^{-s\beta\Lambda_i^0}) - \sum_{i;s=\pm} \ln(1 + e^{-\beta\Lambda_i^s}), \quad (\text{S11})$$

where  $\Lambda_i^0$ ,  $\Lambda_i^+$ , and  $\Lambda_i^-$  are the eigenvalues of  $A$ ,  $Q_1 = BA^{-1}B + M$ , and  $Q_2 = -BA^{-1}B + M^*$ , respectively.

### B. Effect of imbalance between inner and outer layers

We have also performed numerical simulations by assuming different hybridizations or chemical potentials for the inner and two outer layers. Figure S1(a) shows  $T_c$  as a function of  $\eta = V_{\text{outer}}/V_{\text{inner}}$  for three typical values of  $V = V_{\text{inner}}$ . We find  $T_c$  decreases rapidly as  $\eta$  decreases from unity and drops to zero as  $\eta$  approaches zero. The latter reflects the key role of the outer layers in causing the superconductivity. Figure S1(b) plots  $T_c$  as a function of  $\eta' = \mu_{\text{outer}}/\mu_{\text{inner}}$  for a fixed  $\mu_{\text{inner}} = -1.3$  and the same values of  $V$ . We see  $T_c$  decreases as  $\eta'$  decreases for small  $V$  but remains less affected for large  $V$ .

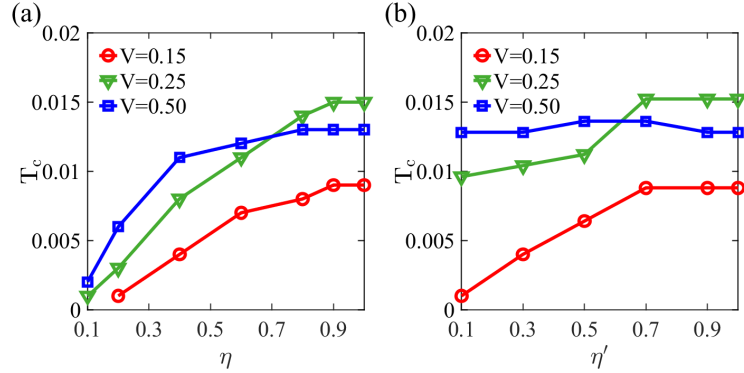


FIG. S1: Evolution of  $T_c$  as functions of (a)  $\eta = V_{\text{outer}}/V_{\text{inner}}$  and (b)  $\eta' = \mu_{\text{outer}}/\mu_{\text{inner}}$  for three typical values of  $V = V_{\text{inner}}$  with  $\mu_{\text{inner}} = -1.3$  and  $J = 0.5$ .

### C. Derivation of the Ginzburg-Landau free energy

The GL free energy density is related to the effective action by  $f_{\text{GL}} = S_{\text{eff}}/\beta N$ . To simplify the derivation, we treat  $t_{\perp}$  as a perturbation such that

$$f_{\text{GL}} = f_{\text{GL}}^{(0)} + f_{\text{GL}}^{(2)} + O(t_{\perp}^4). \quad (\text{S12})$$

For  $t_{\perp} = 0$ , Eq. (S7) gives

$$f_{\text{GL}}^{(0)} = \frac{8}{3JN} \sum_{ia} |\Delta_i^a|^2 - \frac{1}{\beta N} \sum_n \text{Tr} \ln(-i\omega_n + O_1) - \frac{1}{\beta N} \sum_n \text{Tr} \ln(-i\omega_n + O_2). \quad (\text{S13})$$

Since  $\Delta_i^a$  only enter  $M$  and  $M^*$ , we may further make the expansion:

$$\begin{aligned} \text{Tr} \ln(-i\omega_n + O_1) &= \text{Tr} \ln \begin{pmatrix} -i\omega_n + A & B \\ B & -i\omega_n \end{pmatrix} - \frac{1}{2} \text{Tr}(P_1 M)^2 - \frac{1}{4} \text{Tr}(P_1 M)^4, \\ \text{Tr} \ln(-i\omega_n + O_2) &= \text{Tr} \ln \begin{pmatrix} -i\omega_n - A & -B \\ -B & -i\omega_n \end{pmatrix} - \frac{1}{2} \text{Tr}(P_2 M^*)^2 - \frac{1}{4} \text{Tr}(P_2 M^*)^4, \end{aligned} \quad (\text{S14})$$

where

$$P_1 = \begin{pmatrix} P_+ & 0 & 0 \\ 0 & P_- & 0 \\ 0 & 0 & P_+ \end{pmatrix}, \quad P_2 = \begin{pmatrix} P_- & 0 & 0 \\ 0 & P_+ & 0 \\ 0 & 0 & P_- \end{pmatrix}, \quad P_{\pm} = \frac{1}{-i\omega_n + \mathcal{V}(i\omega_n \pm T)^{-1}\mathcal{V}}. \quad (\text{S15})$$

This gives the free energy density (up to a constant):

$$\begin{aligned} f_{\text{GL}}^{(0)} &= \frac{8}{3JN} \sum_{ia} |\Delta_i^a|^2 + \frac{1}{\beta N} \sum_n \text{Tr} [(P_- M_+^* P_+ M_+)^2 + (P_- M_-^* P_+ M_-)^2 + 2P_- M_+^* P_+ M_+ \\ &\quad + 2P_- M_-^* P_+ M_- + P_- M_+^* P_+ M_+ P_- M_-^* P_+ M_- + P_- M_+^* P_+ M_- P_- M_-^* P_+ M_+]. \end{aligned} \quad (\text{S16})$$

Assuming spatially uniform order parameters,  $(M_a)_{ii} = \Delta_i^a = \Delta^a$ , the above formula can be simplified to

$$f_{\text{GL}}^{(0)} = c'_1 (|\Delta^+|^2 + |\Delta^-|^2) + c_2 (|\Delta^+|^2 + |\Delta^-|^2)^2 = c'_1 \Psi^\dagger \Psi + c_2 (\Psi^\dagger \Psi)^2, \quad (\text{S17})$$

where  $\Psi \equiv (\Delta^+, \Delta^-)^T$  and

$$c'_1 = \frac{8}{3J} + \frac{2}{\beta N} \sum_n \text{Tr}(P_+ P_-), \quad c_2 = \frac{1}{\beta N} \sum_n \text{Tr}(P_+ P_- P_+ P_-). \quad (\text{S18})$$

For  $c'_1 < 0$  and  $c_2 > 0$ ,  $f_{\text{GL}}^{(0)}$  is minimized at  $\Psi^\dagger \Psi = -c'_1/2c_2$ .

To obtain  $f_{\text{GL}}^{(2)}$ , we expand the effective action (S3) to  $O(t_{\perp}^2)$  and obtain

$$f_{\text{GL}}^{(2)} = -\frac{2t_{\perp}^2}{\beta N} \sum_n \text{Tr} [P_-^2 M_+^* P_+^2 M_+ + P_-^2 M_-^* P_+^2 M_+ P_-^2 M_+^* P_+^2 M_- + P_-^2 M_-^* P_+^2 M_-], \quad (\text{S19})$$

which, for uniform order parameters  $\Delta^a$ , reduces to

$$f_{\text{GL}}^{(2)} = -2t_{\perp}^2 c_3 [|\Delta^+|^2 + |\Delta^-|^2 + (\bar{\Delta}^- \Delta^+ + c.c.)] \quad (\text{S20})$$

with

$$c_3 = \frac{1}{\beta N} \sum_n \text{Tr}(P_+ P_+ P_- P_-). \quad (\text{S21})$$

Putting together, we get the approximate GL free energy density:

$$f_{\text{GL}} = c_1 \Psi^\dagger \Psi + c_2 (\Psi^\dagger \Psi)^2 - h \Psi^\dagger \sigma_x \Psi, \quad (\text{S22})$$

where  $c_1 = c'_1 - h$  and  $h = 2t_{\perp}^2 c_3$  plays the role of a transverse magnetic field along the  $x$  direction. Introducing the pseudospin  $\mathcal{T}^{\Delta} = \frac{1}{2} \Psi^\dagger \boldsymbol{\sigma} \Psi$  gives Eq. (4) in the main text.

To find the global minimum of Eq. (S22), we write explicitly,  $-h \Psi^\dagger \sigma_x \Psi = -2h|\Delta^+||\Delta^-| \cos(\theta^+ - \theta^-)$ , which is nothing but the Josephson coupling energy of two superconducting layers. Minimizing the free energy with respect to the phase difference  $\Delta\theta \equiv \theta^+ - \theta^-$  yields the solution  $\Delta\theta = 0$  for  $h > 0$  and  $\Delta\theta = \pi$  for  $h < 0$ , at which the GL free energy density becomes

$$f_{\text{GL}} = c_1 (|\Delta^+|^2 + |\Delta^-|^2) + c_2 (|\Delta^+|^2 + |\Delta^-|^2)^2 - 2|h||\Delta^+||\Delta^-|, \quad (\text{S23})$$

with the solution:

$$|\Delta^+| = |\Delta^-| = \begin{cases} \Delta_0 \equiv \sqrt{\frac{|h| - c_1}{4c_2}}, & c_1 < |h| \\ 0, & c_1 \geq |h| \end{cases}. \quad (\text{S24})$$

Our numerical simulations of the current trilayer model always find the solution  $\Delta\theta = 0$  ( $h > 0$ ) at low temperatures. Expanding Eq. (S22) around  $|\Delta^+| = |\Delta^-| = \Delta_0$  and  $\Delta\theta = 0$  yields

$$\delta f_{\text{GL}} = 4c_2\Delta_0^2 (|\Delta^+| + |\Delta^-| - 2\Delta_0)^2 + h (|\Delta^+| - |\Delta^-|)^2 + h\Delta_0^2 (\theta^+ - \theta^-)^2, \quad (\text{S25})$$

indicating strong Gaussian fluctuations of  $|\Delta^+| - |\Delta^-|$  and  $\theta^+ - \theta^-$  proportional to  $h^{-1/2}$ .

#### D. Derivation of the Josephson effect

To study the Josephson effect, we introduce a scalar potential  $\phi_a(\tau)$  for two outer layers relative to the inner layer and take into consideration the imaginary time dependence of the global  $\theta^a(\tau)$  inside the BKT phase. For simplicity, we ignore their spatial dependence on each layer. These yield additional dynamics of  $\theta^a(\tau)$  with the effective action:

$$\begin{aligned} S_\theta &= \int_0^\beta d\tau \left[ \sum_{ais} \bar{c}_{ais} (i\partial_\tau \theta^a + ie\phi_a) c_{ais} + \sum_{ais} \bar{d}_{ais} (i\partial_\tau \theta^a + ie\phi_a) d_{ais} - 2h \sum_i |\Delta^+| |\Delta^-| \cos(\theta^+ - \theta^-) \right] \\ &= \int_0^\beta d\tau \left[ i \sum_a \mathcal{N}_a (\partial_\tau \theta^a + e\phi_a) - 2U \cos(\theta^+ - \theta^-) \right], \end{aligned} \quad (\text{S26})$$

where  $\mathcal{N}_a = \sum_{is} (\bar{d}_{ais} d_{ais} + \bar{c}_{ais} c_{ais})$  and  $U = h \sum_i |\Delta^+| |\Delta^-|$ . The above action can be further split into two terms,  $S_\theta = S_0 + S_J$ , with

$$\begin{aligned} S_0 &= \frac{i}{2} \int_0^\beta d\tau \mathcal{N} (\partial_\tau \bar{\theta} + e\bar{\phi}), \\ S_J &= \int_0^\beta d\tau \left[ \frac{i\Delta\mathcal{N}}{2} (\partial_\tau \Delta\theta + e\Delta\phi) - 2U \cos \Delta\theta \right], \end{aligned} \quad (\text{S27})$$

where we have defined  $\mathcal{N} = \sum_a \mathcal{N}_a$ ,  $\bar{\theta} = \sum_a \theta^a$ ,  $\bar{\phi} = \sum_a \phi_a$ , and  $\Delta\mathcal{N} = \mathcal{N}_+ - \mathcal{N}_-$ ,  $\Delta\theta = \theta^+ - \theta^-$ ,  $\Delta\phi = \phi_+ - \phi_-$ . Obviously,  $S_0$  is not relevant, while  $S_J$  describes the dynamics of the phase difference and is responsible for the Josephson effect. Minimizing  $S_J$  with respect to  $\Delta\mathcal{N}$  and  $\Delta\theta$  yields the equations of motion:

$$\partial_\tau \Delta\theta = -e\Delta\phi, \quad i\partial_\tau \Delta\mathcal{N} = 4U \sin \Delta\theta \quad (\text{S28})$$

After the Wick's rotation  $\tau \rightarrow it$ ,  $\phi \rightarrow -i\phi$ , we obtain

$$\partial_t \Delta\theta = -e\Delta\phi, \quad \partial_t \Delta\mathcal{N} = 4U \sin \Delta\theta \quad (\text{S29})$$

where  $\Delta\phi = \phi_+ - \phi_-$  is the voltage difference between two outer layers. The Josephson current is then

$$I_{-\rightarrow+} = (-e) \frac{d\mathcal{N}_+}{dt} = -\frac{e}{2} \frac{d(\Delta\mathcal{N})}{dt} = -2eU \sin \Delta\theta = 2eU \sin(e\Delta\phi t + \alpha), \quad (\text{S30})$$

where  $\alpha$  is a constant offset. We have therefore a characteristic oscillation frequency  $\omega_J = e\Delta\phi/\hbar$ , half that of the usual ac Josephson effect for intralayer pairing. This can be easily understood, because for interlayer pairing, a phase change  $d_{ais} \rightarrow d_{ais} e^{i\theta^a}$  yields  $\Delta_i^a \rightarrow \Delta_i^a e^{i\theta^a}$ , while for intralayer pairing, it yields  $\Delta_i^a \rightarrow \Delta_i^a e^{2i\theta^a}$ .

---

\* yifeng@iphy.ac.cn